MODELLING AND SIMULATION OF AIRFLOW IN AN INCLINED BIFURCATED TRACHEA

Esam A. Alnussairy[1, a)], Ahmed Bakheet [2], Norzieha Mustapha [3] and Norsarahaida Amin[4]

[1] Department of Mathematics, College of Computer Science and Mathematics, Wasit University, Iraq.

[2] Department of Mathematics, College of Science, Mustansiriyah University, Baghdad, Iraq.

[3] Computer Science and Mathematics, Universiti Teknologi MARA UiTM Kelantan,18500 Machang, Kelantan, Malaysia

[4] Department of Mathematical Sciences, Faculty of Science, University Technology Malaysia,

[a)] Corresponding author: eahmed@uowasit.edu.iq.

ABSTRACT: *The effect of horizontal sleeping position on the health of some patients with breathing problems still needs to be clarified. A new update mathematical model for simulating the unsteady airflow inside a bifurcated trachea for various Reynolds numbers and inclination angles is determined. The governing unsteady equations of motion, consisting of two-dimensional Navier-Stokes equations, nonlinear and non-homogenous are derived and numerically solved using the finite difference Marker and Cell (MAC) method. A numerical code based on the Matlab platform is developed to calculate specifically, in addition to other flow characteristics, the pressure distribution and the streamlines which are missing in most previous works in this area. The results for axial velocities at a horizontal situation show good agreement with both numerical and other experimental findings. New results show that an increase in the inclination angle diminishes the pressure drop inside the main and a bifurcated trachea, Sleeping in a horizontal position leads to a negative effect for many patients. Consequently, the bed should be positioned at the angle between 30^o and 45^o. The excellent features of these results suggest that the proposed model-based procedure may contribute towards the development of more accurate and effective inclined bed therapy (IBT*).

Keywords: Numerical simulation; bifurcated trachea; pressure correction; Inclined Bed Therapy (IBT)

1. INTRODUCTION

Mathematical models of a bifurcated trachea are essential for the development of biomedical engineering. Currently, the understanding of airflow through human airways is gaining much research attention either from a numerical viewpoint or from the experimental design. Recently, comprehensive understanding and prediction of phenomena in physiology demanded and life sciences accurate mathematical models with numerical simulation methods. This is particularly true for realizing (IBT) inclined bed therapy, which is a perfectly normal remedy for many health problems without using harmful chemicals or any substances in the patients' body. IBT is a new therapy presented by Andrew Fletcher [1] seemed promising. IBT therapy expands the capacity of the body to perform without externally infused of synthetic chemicals. It is beneficial for numerous illnesses linked with breathing problems such as snoring, asthma, mild sleep apnea and chronic obstructive pulmonary disease (COPD) [2-4]. The inspiratory flow rates in the human respiratory system depend on the strength of physical activity. The range of Reynolds numbers (*Re*) of airflow in human trachea range from 800-9300 depend on quiet or heavy breathing [5]. Numerically simulated of respiratory flow patterns introduced in [6] to study the inhalation and the exhalation through a single bifurcation for Reynolds numbers 50-4500. Calay *et al*. [7] introduced a numerically simulated of respiratory flow patterns through the trachea and main bronchi at resting with *Re* = 1750 and at maximal exercising with *Re* = 4600. Definitely, the understanding of airflow in the human trachea is an alternative method to support the treatment of patients suffering from breathing complications. Thus, a mathematical model depicting the dynamics of airflow movement in the trachea in terms of governing equations of motion is valuable. many computational fluid dynamics researchers to investigate the air flow through the trachea have been carried out. Li *et al*. [8, 9] investigated steady laminar and transient air flow field and particle deposition in a trachea with *Re* = 1201 for breathing in resting conditions. The numerical results of velocities are compared with the experimental results of Zhao and Lieber [10]. Their mathematical model with steady, laminar, incompressible, and three-dimensional airflow in rigid airway was developed. Commercial software based on finite volume used to simulate their model. Liu *et al*. [11] utilized a child model to investigate the impacts of physiological features on the airflow patterns and nanoparticle deposition in the upper respiratory tracts. Their model in three-dimensions involved the mouth cavity, larynx, pharynx, trachea and bronchial and is considered to be incompressible, laminar and steady with a low Reynolds number. A mathematical model of airflow in the upper respiratory tract described in [12, 13] considering the air as incompressible and Newtonian with constant density and viscosity. The results obtained using a finite element analysis and (COMSOL software) then the simulation results compared with those in [12] from an analytical calculation based on Fourier series. Alnussairy *et al*. [14, 15] investigated the inclination angle dependence on the unsteady airflow in the main trachea by developing a 2D mathematical model (channel and tube) using two methods analytically and numerically. The exact and numerical solutions are achieved using the Bromwich integral and MAC method. Their results for axial velocity at the horizontal position of the trachea ($\theta = 0^o$) is compared with the observation of Kongnuan and Pholuang [8] and Zhao and Lieber [6] respectively. Chen *et al.* [16] carried out experiments and simulation to investigate fiber deposition in a single horizontal bifurcation under different steady inhalation conditions. The flow was applied incompressible, Newtonian, laminar and fully developed, a parabolic velocity distribution at the inlet. The governing equations for their model solved using Fluent software. Many types

of research [7, 8, 9, 11, 13, 16] achieved results worth using commercial simulation software and using a given inlet velocity and pressure with proper boundary conditions. These software programs are often very expensive and not easily available. Moreover, the pressure distribution in the tracheal segment is unknown parameter needs an appropriate method for calculation. To avoid this limitation, following [17, 18, 19]. Yet, no systematic mathematical model is developed to simulate precisely the inclination angle dependent unsteady air flow inside the human trachea. No one investigated the effect of the inclination angle on the airflow in the trachea and main bronchi although the inclined angle position is one of the most important parameters that affect such flow.

This paper investigates the effect of inclination angle position on the airflow pattern in the trachea and main bronchi under resting and normal breathing conditions using Marker and cell method, which is helpful because the pressure boundary conditions at the inlet and outlet are not needed. The velocity vector is identified and the results are achieved with the desired degree of accuracy.

2. Governing Equations

Consider air flow model in the tracheal lumen is treated as 2D unsteady, nonlinear, incompressible (low Mach number, M = 0.1, [7], laminar, Newtonian fluid with constant a kinematic viscosity $\nu = \mu/\rho$. The governing momentum and continuity, conservation equations in dimensionless of the axisymmetric air flow in the cylindrical polar coordinate system (r, z) are written as:

$$\frac{1}{r}\frac{\partial}{\partial r}(ru)+\frac{\partial}{\partial z}(w)=0 \tag{1}$$

$$\frac{\partial w}{\partial t}+\frac{\partial (wu)}{\partial r}+\frac{\partial w^2}{\partial z}+\frac{wu}{r}= \frac{\partial p}{\partial z}+\frac{1}{\mathrm{Re}}\left(\frac{1}{r}\frac{\partial w}{\partial r}(r\frac{\partial w}{\partial r})+\frac{\partial^2 w}{\partial z^2}\right)+\frac{\sin(\theta)}{Fr} \tag{2}$$

$$\frac{\partial u}{\partial t}+\frac{\partial u^2}{\partial r}+\frac{\partial (uw)}{\partial z}+\frac{u^2}{r}= -\frac{\partial p}{\partial r}+\frac{1}{\mathrm{Re}}\left(\frac{1}{r}\frac{\partial u}{\partial r}(r\frac{\partial u}{\partial r})-\frac{u}{r^2}+\frac{\partial^2 u}{\partial z^2}\right)-\frac{\cos(\theta)}{Fr} \tag{3}$$

where $Re = \rho U_0 R_0/\mu$, $Fr = U_0/\sqrt{gR_0}$, $t, \rho, \mu, p, U_0, R_0$ is the Reynolds number, the Froud number, the time, density, viscosity of air, pressure, an average of the velocity at the inlet and the radius of the trachea respectively. The axial and radial equations of momentum (2), (3) are imposed with a gravitational force parameter g. The angle θ is the slope between the horizontal direction z and the direction of the trachea [15]. The functions $R_1(z)$ and $R_2(z)$ which represent the outer and inner wall of the trachea respectively [cf. Fig.1] is given by:

$$R_1(z)=\begin{cases}1, & 0\le z<z_1\\ 1+r_1-\sqrt{r_1^2-(z-z_1)^2}, & z_1\le z<z_2\\ 2r_1'sec\beta+(z-z_2)tan\beta, & z_2\le z<z_{\max}\end{cases} \tag{4}$$

$$R_2(z)=\begin{cases}0, & 0\le z<z_3\\ \sqrt{r_2^2-(z-z_3-r_2)^2}, & z_3\le z<z_3+r_2(1-sin\beta)\\ r_2cos\beta+z_4, & z_3+r_2(1-sin\beta)\le z<z_{\max}\end{cases} \tag{5}$$

Where

$$r_1=\frac{(1-2r_1'\sec\beta)}{(\cos\beta-1)};\ r_2=\frac{(z_3-z_2)\sin\beta}{1-\sin\beta};$$

$$z_2=z_1+(1-2r_1'\sec\beta)\frac{\sin\beta}{\cos\beta-1};$$

$$z_3=z_2+0.5\ ;\ z_4=(z-(z_3+r_2(1-\sin\beta)))\tan\beta$$

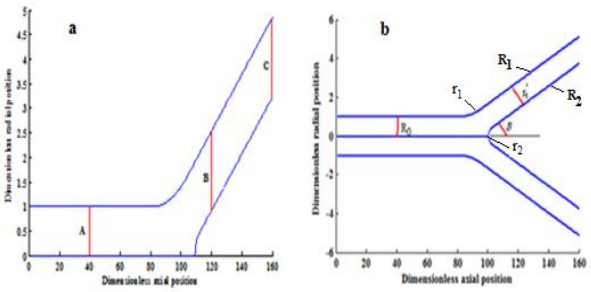

Figure 1. (a) Geometry for a single bifurcated trachea (b) Axisymmetric geometry for a bifurcated trachea

2.1 Initial and Boundary Conditions

The velocity components of the airflow stream on the trachea wall should be zero at the rigid wall (no-slip condition). A maximum velocity of airflow is assumed to be fully developed parabolic velocity profile with at the inlet corresponds to the Poiseuille flow [15, 16, 20] of the tracheal lumen yields:

$$w(r,z,t)=U_{\max}\left(1-\left(\frac{r}{R}\right)^2\right), u(r,z,t)=0 \tag{6}$$

at $z = 0$, where $U_{\max}=2U_0$

The boundary and initial conditions of the problem is set as:

$$w(r,z,t)=0=u(r,z,t) \text{ on } r=R_1(z) \text{ and } r=R_2(z), z_3\le z\le z_{\max} \tag{7}$$

$$\frac{\partial w(r,z,t)}{\partial r}=0, \text{ on } r=0,\ 0\le z\le z_3 \tag{8}$$

$$w(r,z,0)=0,\ u(r,z,0)=0,\ p(r,z,0)=0 \text{ for } z>0 \tag{9}$$

2.2 Radical Transformation

The radical transformation is introduced:

$$\xi=\frac{r-R_2(z)}{R(z)}, R(z)\neq 0, \tag{10}$$

where $R(z)=R_1(z)-R_2(z)$, which has the influence of immobilizing the tracheal wall in the transformed coordinate ξ. Using the radial transformation in equation (10). Therefore, the Equations (1)-(3) takes the form:

$$(\xi R+R_2)\frac{\partial w}{\partial z}-\frac{\xi R+R_2}{R}\left(\xi\frac{\partial R}{\partial z}+\frac{\partial R_2}{\partial z}\right)\frac{\partial w}{\partial \xi}+ \frac{\partial (u(\xi R+R_2)/R)}{\partial \xi}=0 \tag{11}$$

$$\frac{\partial w}{\partial t} = -\frac{\partial p}{\partial z} + \frac{1}{R}\left(\xi\frac{\partial R}{\partial z} + \frac{\partial R_2}{\partial z}\right)\frac{\partial p}{\partial \xi} + \text{Con}w + \frac{1}{\text{Re}}\text{Diff}w + \frac{\sin\theta}{\text{Fr}} \quad (12)$$

$$\frac{\partial u}{\partial t} = -\frac{1}{R}\frac{\partial p}{\partial \xi} + \text{Con}u + \frac{1}{\text{Re}}\text{Diff}u - \frac{\cos\theta}{\text{Fr}} \quad (13)$$

where

$$\text{Con}w = -\frac{1}{R}\frac{\partial(uw)}{\partial\xi} - \frac{uw}{\xi R + R_2} - \frac{\partial w^2}{\partial z} + \frac{1}{R}\left(\xi\frac{\partial R}{\partial z} + \frac{\partial R_2}{\partial z}\right)\frac{\partial w^2}{\partial \xi} \quad (14)$$

$$\text{Diff}w = \frac{\partial^2 w}{\partial z^2} - \frac{2}{R}\left(\xi\frac{\partial R}{\partial z} + \frac{\partial R_2}{\partial z}\right)\frac{\partial^2 w}{\partial z\,\xi} + \frac{1}{R^2}\left(1 + \left(\xi\frac{\partial R}{\partial z} + \frac{\partial R_2}{\partial z}\right)^2\right)\frac{\partial^2 w}{\partial \xi^2} + \frac{1}{R}\left(\frac{1}{\xi R + R_2} + \frac{2}{R}\frac{\partial R}{\partial z}\left(\xi\frac{\partial R}{\partial z} + \frac{\partial R_2}{\partial z}\right) - \left(\xi\frac{\partial^2 R}{\partial z^2} + \frac{\partial^2 R_2}{\partial z^2}\right)\right)\frac{\partial w}{\partial \xi} \quad (15)$$

$$\text{Con}u = -\frac{1}{R}\frac{\partial u^2}{\partial \xi} - \frac{u^2}{\xi R + R_2} - \frac{\partial(uw)}{\partial z} + \frac{1}{R}\left(\xi\frac{\partial R}{\partial z} + \frac{\partial R_2}{\partial z}\right)\frac{\partial(uw)}{\partial \xi} \quad (16)$$

$$\text{Diff}u = \frac{\partial^2 u}{\partial z^2} - \frac{2}{R}\left(\xi\frac{\partial R}{\partial z} + \frac{\partial R_2}{\partial z}\right)\frac{\partial^2 u}{\partial z\,\xi} + \frac{1}{R^2}\left(1 + \left(\xi\frac{\partial R}{\partial z} + \frac{\partial R_2}{\partial z}\right)^2\right)\frac{\partial^2 u}{\partial \xi^2} + \frac{1}{R}\left(\frac{1}{\xi R + R_2} + \frac{2}{R}\frac{\partial R}{\partial z}\left(\xi\frac{\partial R}{\partial z} + \frac{\partial R_2}{\partial z}\right) - \left(\xi\frac{\partial^2 R}{\partial z^2} + \frac{\partial^2 R_2}{\partial z^2}\right)\right)\frac{\partial u}{\partial \xi} - \frac{u}{(\xi R + R_2)^2} \quad (17)$$

Likewise, the initial and boundary conditions (6) – (9) are also transformed accordingly using equation (10), and $\xi \in [0,1]$.

$$w(\xi,z,t) = U_{\max}\left(1-\xi^2\right), u(\xi,z,t) = 0 \text{ for } z = 0 \quad (18)$$

$$w(\xi,z,t) = 0 = u(\xi,z,t) \text{ on } \xi = R_1(z) \text{ and } \xi = R_2(z), z_3 \le z \le z_{\max} \quad (19)$$

$$\frac{\partial w(\xi,z,t)}{\partial \xi} = 0, \text{ on } \xi = 0,\ 0 \le z \le z_3 \quad (20)$$

$$w(\xi,z,0) = 0,\ u(\xi,z,0) = 0,\ p(\xi,z,0) = 0 \text{ for } z > 0 \quad (21)$$

2.3 Method of Solution and Discretization Procedure

The above unsteady governing equations (11) - (13) are discretized using Marker and Cell (MAC) method [21]. The pressure and velocities are computed at different locations as shown in Figure 2. By defining $\xi = j\Delta\xi,\ z = i\Delta z,\ t = n\Delta t$ and $p(\xi,z,t) = p(j\Delta\xi, i\Delta z,\ n\Delta t) = p^n_{i,j}$, where n refers to the time t, Δt is the increment of time, while Δz, $\Delta\xi$ being the length and width of the *(i,j)* cell of the control volume respectively.

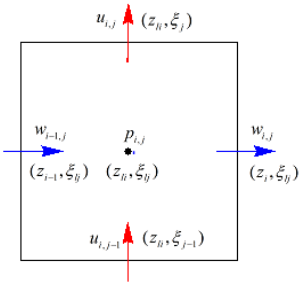

Figure 2. MAC Cell Method

4.2. Discretization of Governing Equations

The discretization of the continuity and momentum equations are performed at the (i, j) cell to obtain:

$$(\xi_{lj}R^n_{li} + R^n_{2li})\left(\frac{w^n_{i,j} - w^n_{i-1,j}}{\Delta z}\right) - \frac{\xi_{lj}R^n_{li} + R^n_{2li}}{R^n_{li}}\left(\xi_{lj}\left(\frac{\partial R}{\partial z}\right)^n_{li} + \left(\frac{\partial R_2}{\partial z}\right)^n_{li}\right)\left(\frac{w_{at} - w_{ab}}{\Delta\xi}\right) + \frac{(\xi_j R^n_i + R^n_{2i})u^n_{i,j} - (\xi_{j-1}R^n_i + R^n_{2i})u^n_{i,j-1}}{R^n_i\Delta\xi} = 0 \quad (22)$$

where

$$w_{at} = \frac{w^n_{i,j} + w^n_{i-1,j} + w^n_{i-1,j+1} + w^n_{i,j+1}}{4} \quad (23)$$

$$w_{ab} = \frac{w^n_{i,j} + w^n_{i-1,j} + w^n_{i-1,j-1} + w^n_{i-1,j-1}}{4} \quad (24)$$

$$\xi_{lj} = \xi_j - \frac{\Delta\xi}{2},\ R^n = R(z_{lj}),\ z_{lj} = z_i - \frac{\Delta z}{2}$$

and

$$\frac{w^{n+1}_{i,j} - w^n_{i,j}}{\Delta t} = \left(\frac{p^n_{i,j} - p^n_{i+1,j}}{\Delta z}\right) + \frac{1}{R^n_i}\left(\xi_{lj}\left(\frac{\partial R}{\partial z}\right)^n_i + \left(\frac{\partial R_2}{\partial z}\right)^n_i\right)\left(\frac{p_t - p_b}{\Delta\xi}\right) + wcd^n_{i,j} \quad (25)$$

$$wcd^n_{i,j} = \text{Con}w^n_{i,j} + \frac{1}{\text{Re}}\left(\text{Diff}w^n_{i,j}\right) + \frac{\sin\theta}{Fr} \quad (26)$$

$$\frac{u^{n+1}_{i,j} - u^n_{i,j}}{\Delta t} = -\frac{1}{R^n_{lj}}\left(\frac{p^n_{i,j} - p^n_{i,j+1}}{\Delta\xi}\right) + ucd^n_{i,j} \quad (27)$$

where $ucd^n_{i,j} = \text{Con}u^n_{i,j} + \frac{1}{\text{Re}}\left(\text{Diff}u^n_{i,j}\right) - \frac{\cos\theta}{Fr}$ (28)

where $\text{Con}u^n_{i,j}$ and $\text{Diff}u^n_{i,j}$ are convective and diffusive terms of the *u*- momentum equation at n[th] time level at the (i, j) th cell. The terms are differences in the similar terms manner as in the *w*- equation of momentum. The complete numerical procedure already discussed in Alnussairy *et al* [15]. By using the result of *w*-velocity, volumetric flow rate (Q) and resistance to flow (λ) are described as:

$$Q^n_i = 2\pi(R^n_i)^2\int_0^1 \xi_j(w_{i,j})d\xi_j \quad (29)$$

$$\lambda = \frac{|\Delta p|}{Q^n_i} \quad (30)$$

3. DISCUSSIONS

The numerical and simulations are performed using $\mu = 1.79\times10^{-5}$ pa.s, $\rho = 1.225$ kg.m^{-3}, $g = 9.8$ m.s^{-2}, $R_0 = 0.01085$ m, $r_1^{'} = 0.0065$, (radius of left bronchi), z_1=0.092m, $\beta = 30^o$ (angle of branching between left branch and main branch) [5, 7], $\Delta z = 0.1$ and $\Delta\xi = 0.025$.the Reynolds numbers of rest and normal conditional breathing is taken in the range of 800 to 2000 and also tracheal length $z_{max} = 0.16$ m in nondimensional. The solutions are generated by using a staggered grid of size 1600×40 at constant $Fr = 0.27$, $Re = 1200$ and $U_0 = 85\times10^{-2}$ m.s^{-1}. The pressure-based a finite-difference approximation is used to solve the unsteady governing PDE equations of motion. The results are found after the steady state is achieved in the simulation when the dimensionless $t = 80$. The pressure is computed to determine the velocity after solving the momentum equations.

The velocity field is plotted for every slice to generate a complete description of the flow patterns in the trachea during resting and normal breathing with varying *Re*. The accuracy of the proposed method is validated with existing experimental data and numerical studies (Schroter and Sudlow [6]); Calay *et al.*[7]). Figure 3 compares the variation of axial velocity dependent radial position obtained by the present model with other findings for *Re* = 1570 and $\theta = 0^o$. The *w*-velocity at slice A (z = 4) revealed a parabolic pattern. In addition, the laminar flow exhibited a maximum velocity in the central region and decreased to 0 close to the walls (Schroter and Sudlow,[6]). Conversely, the *w*-velocity at slice B (z = 12) is highly skewed toward the inner wall and lowered in the outer wall of the single bifurcation. This is in a good agreement with the findings of Calay *et al.*[7] on *w*-velocity for different axial positions in main and single bifurcated trachea.

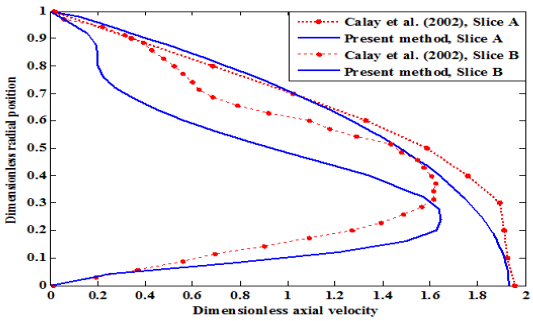

Figure 3:. Comparison of the axial velocity with others for *Re* = 1570 when $\theta = 0^o$

It calculated value of axial velocity in the horizontal straight trachea ($\theta = 0^o$) for *Re* = 700 and slice B is compared with the experimental results of Schroter and Sudlow [6] as shown in Figure 4. The *w*-velocity near the outer wall is very slow. Thus, the velocity distribution is low in the outer and high in the inner wall.

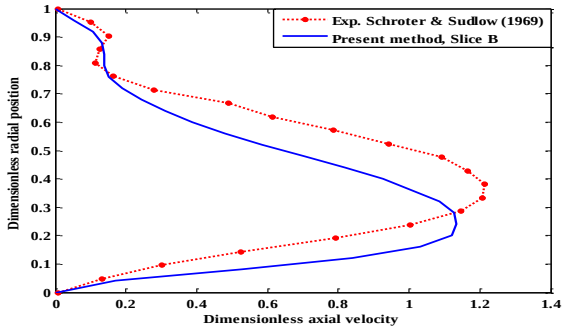

Figure 4: Comparison of the *w*-velocity in a bifurcated trachea position (slice B) with *Re* = 700 and $\theta = 0$

Figure 5 presents the axial velocity dependent radial position at different axial locations for *Re* = 1200 and $\theta = 0^o$. At $z = 4$ (slice A) the *w*-velocity revealed the parabolic shape inside the parent due to the prescribed boundary condition. However, the velocity distributions after the flow get divided inside the daughter tube at other axial locations. The velocity at location $z = 12$ (slice B) near the outer wall is very slow, thus the velocity distribution is low in the outer and high in the inner wall. At z = 13.5 the velocity gradient is decreased very rapidly near the inner wall and it started rising in the outer wall to become M-shape. A typical M-shape, velocity is revealed at z = 16 (slice C). Furthermore, the velocity near the outer wall is high and reversed. This indicates the appearance of backflow separation near the outer wall for all values of *Re*.

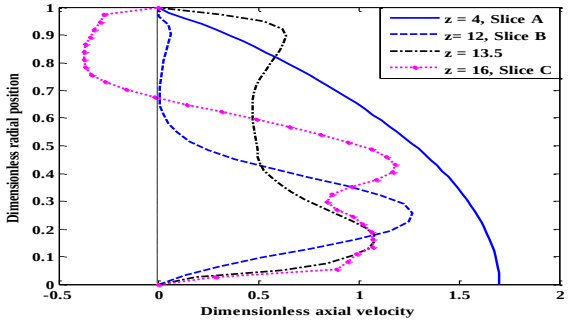

Figure 5: Variation of *w*-velocity for different position of *z* with *Re* = 1200 and $\theta = 0^o$.

Figure 6 shows the *w*-velocity for different inclination angle position with fixed *Re* = 1200, *Fr* = 0.27 and $z = 12$ (slice B). An increase in the angle of inclination (from 0^o to 45^o) is found to enhance the airflow velocity. These results are in an agreement with the observation of Vliet *et al.* [3] & Ragavan *et al.* [4].

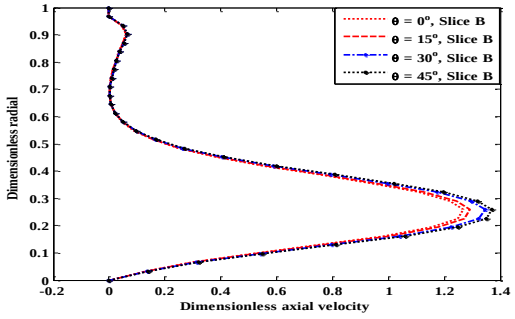

Figure 6.: Variation of *w*-velocity for variance θ with Re = 1200, *Fr* = 0.27 and axial position (slice B)

In human anatomy, pressure loss (wall) in the bifurcation airways plays a vital role in the process of respiration. The change of the pressure loss in human lung airways and alveoli is the driving force in the respiratory system. Thus, it is necessary to understand the effect of inclination angle and boundary condition on the pressure loss.

Figures 7 demonstrate the influence of the slope angle of the human trachea on the pressure loss ($\Delta p = p - p_0$), where p_0 signifies the inlet pressure. An increase in the slope angle situation is observed to enhance pressure loss. It is because at a higher angle of inclination the velocity of airflow into the lungs during inhalation is increased. So, the increasing slope angle of the trachea increased the velocity of airflow through the main and the bifurcated trachea to the lungs. This, in turn, generated a greater negative pressure in the lungs. It supported the principle of Bernoulli's, where the pressure exerted by the gas is inversely related to the speed of the gas flow [22].

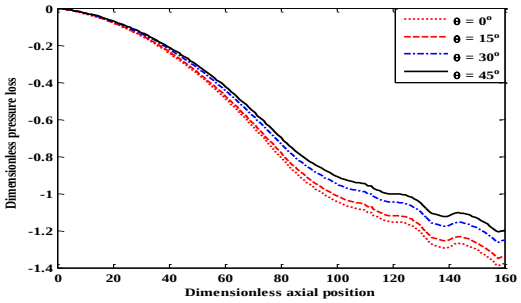

Figure 7: Variation of pressure loss with the axial position for different θ with Re = 1200 and *Fr* = 0.27

Figure 8 presents the axial position-dependent changes in the volumetric flow rate (Q) for different θ at Re = 1200 and Fr = 0.27. For higher slope position the value of Q inside a straight trachea is enhanced. Conversely, the flow rate through the main bronchi is reduced because of the narrowing of the airway branch diameter. Moreover, the influence of slope angle (θ = 15°) is found to be insignificant.

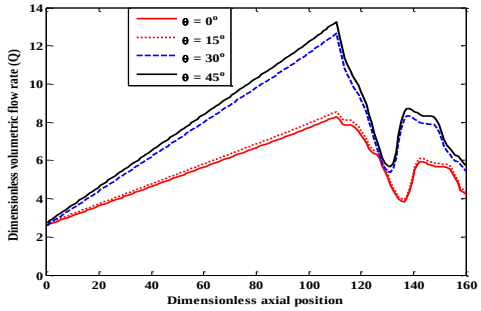

Figure 8: Variation of the volumetric flow rate with the axial position for variance θ with Re =1200 and *Fr* = 0.27

According to Chovancova and Elener [23] flow of resistance in the airways depends on whether the flow is turbulent or laminar on the dimensions of the airway and on the gas viscosity. Therefore, the resistance to flow in a trachea at different θ is shown in Figure 9. It revealed an increase when going down the first bifurcated trachea. This implies a reduction in the airway branch diameter (cross-section area). It is clear that the flow resistance, reduced with increasing slope position of θ.

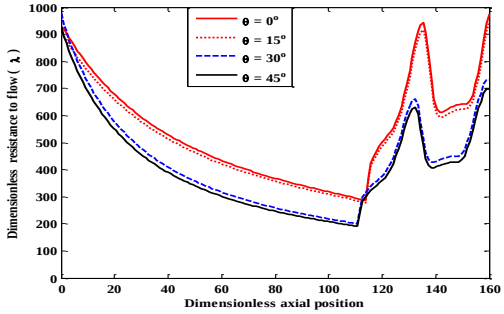

Figure 9: Difference of the resistance to flow with axial position for variance θ with Re = 1200 and *Fr* = 0.27

The understanding of airflow patterns through human trachea is significant to study the aerosolized medication delivery processes and localized diagnostics diseases of the lung. Figure 10 - 11 display axial position dependent streamlines behaviour of airflow for different values of θ. For θ = 0° (Figures 10, 11) it is found that there are regions in the bifurcated trachea where the flow recirculation occurred irrespective of the *Re*. Furthermore, this recirculation is increased in the outer wall at the higher inclination angle of 30° (Figure 11).

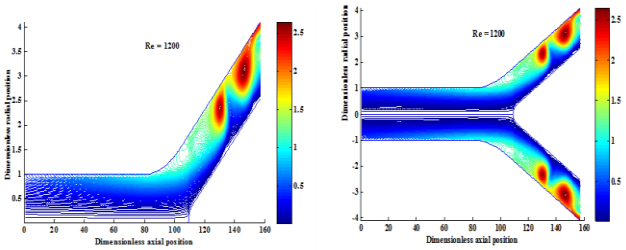

Figure10: Streamline of airflow pattern through main and single bifurcated trachea for Re=1200 at θ = 0°

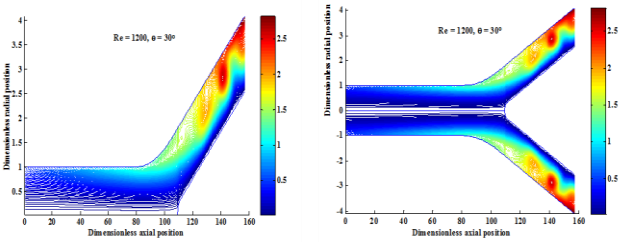

Figure 11: Streamline of airflow pattern through main and single bifurcated trachea for Re= 1200 at θ = 30°

4. CONCLUSION

A symmetric mathematical model is developed and simulated to determine the effect of the slope angle of the airflow through the trachea and main bronchi. The numerical model is simulated by using a MAC method with staggered grids. Increasing the slope angle is found to increase axial velocity, pressure loss, and volumetric flow rate through the main trachea. The resistance to flow (pressure drop) is reduced with the increase of slope angle. The recirculation regions are increased in the outer

wall with a higher slope angle. The sleeping in a horizontal situation leads to a negative influence for many patients. Thus, the slope angle situation between 30^o- 45^o is demonstrated to induce a better influence that may be helpful to patients with chronic obstructive pulmonary disease and other respiratory diseases.

ACKNOWLEDGMENT

The first two authorsthe would like to acknowledge the Ministry of Higher Education (MOHE), Iraq and University Technology Malaysia (UTM) for the financial support for this research.

5. REFERENCES

[1] E. Billen and T. Y. Ting, Inclined bed therapy and diabetes: The Effect of Inclined Bed Therapy on Diabetes Individuals. Available at: http://www.newmediaexplorer.org/sepp/Diabetes_IBT.pdf,2013..

[2] J. A. Rowley, C. McGowen, S. Lareau, B. Fahy, C. Garvey and M. Sockrider, What is Obstructive Sleep Apnea in Adults?. Amer. *J. Respirtory.& Critical care Medicine*, 179, No.12,2009

[3] P. W. Van Vliet, E. R. Ellis and J. Hila, The Effect of Angle and Oscillation on Mucous Simulant Speed in Flexible Tubes. *Physiotherapy Research International*,10, No. 3, pp. 125-133,2005.

[4] J. Ragavan, C. A. Evrensel and P. Krumpe, Interactions of Airflow Oscillation, Tracheal Inclination and Mucus Elasticity Significantly Improve Simulated Cough Clearance. *Chest J*., 137 No. 2, pp. 355-361, 2010.

[5] X. Y. Luo, J. S. Hinton, T. T. Liew, and K. K. Tan, LES Modelling of Flow in a Simple Airway Model. *Medical Eng & Phys* 26, No. 5, pp. 403-413,2004

Figure 11 Streamline of airflow pattern through main and single bifurcated trachea for Re= 1200 at $\theta = 30^o$

[6] R.C. Schroter, and M.F. Sudlow, Flow Patterns in Models of the Human Bronchial Airways. *Respiration Physiol.*, 7, No. 3, pp. 341-55, 1969.

[7] R. K., Calay, J. Kurujareon, and A. E. Holdø, Numerical Simulation of Respiratory Flow Patterns Within Human Lung. *Respiratory Physiol & Neurobiol* 130 No.2, pp. 201-22, 2002..

[8] Z. Li, C. Kleinstreuer, and Z. Zhan, Simulation of Airflow Fields and Microparticle Deposition in Realistic Human Lung Airway Models. Part I: Airflow Patterns. European *J. Mech. - B/Fluids*, 26, No. 5, pp. 632–649, 2007..

[9] Z. Li, C. Kleinstreuer, and Z. Zhang, Particle Deposition in The Human Tracheobronchial Airways Due to Transient Inspiratory Flow Patterns. *J.Aerosol Sci*., 3, No. 6 , pp. 625–644, 2007.

[10] Y. Zhao and B.B. Lieber, Steady inspiratory flow in a model symmetric bifurcation. *J. Biomech. Eng*., 116 , No. 4, pp. 488-496, 1994

[11] Z. Liu, A. Li, X. Xu, and R. Gao. Computational Fluid Dynamics Simulation of Airflow Patterns and Particle Deposition Characteristics in Children Upper Respiratory Tracts. Eng. Appl. Compu. Fluid Mech., 6, No. 4, pp. 556-571,2012.

[12] S. Kongnuan, and J. Pholuang. A Fourier Series-Based Analytical Solution for the Oscillating Airflow In A Human Respiratory Tract. International *J. Pure & Appl. Math*., 78, No. 5, pp. 721–733, 2012.

[13] S. Kongnuan, U. Na-Thakuatung, and J. Pholuang. A comparative of analytical and numerical simulations for the oscillating airflow in a human oral airways. International J. *Pure & Appl Math*, 90, No.3, pp. 321–333, 2014.

[14] E. A. Alnussairy, A. Bakheet, N. Amin. Exact Solution of Two-Dimensional Unsteady Airflow in an Inclined Trachea. *Modern Appl. Sci*. 10, No. 2, pp. 191-200, 2016.

[15] E.A.. Alnussairy, A. Bakheet, N. Mustapha and N. Amin. Numerical model for unsteady airflow in inclined human trachea. In *AIP Conference Proceedings* 1830 (1), 020028 , 2017.

[16] X. Chen, ,W. Zhong, J. Tom, C. Kleinstreuer, Y. Feng, and X. He . Experimental-computational study of fibrous particle transport and deposition in a bifurcating lung model. *Particuology*, 2016.

[17] P. Mandal, and P. K. Mandal, An unsteady analysis of arterial drug transport from half-embedded drug-eluting stent. *Appli. Math. & Comp*., 266, pp. 968-981, 2015.

[18] P. K.. Mandal, Effect of diffusivity on the ransport of drug eluted from drug-eluting stent. International J. Appl. & Compu. Math., pp.1-11. 2015.

[19] N . Mustapha, S. Chakravarty, P.K. Mandal, I. Abdullah, N. Amin, and T. Hayat, A Numerical Simulation of Generalized Newtonian Blood Flow Past A Multiple of Irregular Arterial Stenoses. *Numeric. Meth. for PDE* 27, pp. 960–98, 2011.

[20] F. M. White. *Fluid Mechanics*, Seventh Edition. McGraw-Hill, New York, 270, 2011

[21] F. H. Harlow, and J. E. Welch, Numerical Calculation of Time-Dependent Viscous Incompressible Flow of Fluid with Free Surface, *Phys Fluid*s, 8, No. 12, pp. 2182, 1965.

[22] J. E. Hall, *Guyton and Hall textbook of medical physiology*. Elsevier Health Sciences,(2010), pp. 545-546.

[23] M. Chovancov´a and J. Elcner. The Pressure Gradient in The human Respiratory Tract. *InEPJ Web of Conferences* 67, pp.02047, 2014.